Research Square

Preprints are preliminary reports that have not undergone peer review.
They should not be considered conclusive, used to inform clinical practice,
or referenced by the media as validated information.

Integrated bulk and single-cell transcriptomic profiling identify ILC3s- associated inflammatory signatures in LPS-induced murine pregnancy loss

Yongqin Jia
15178847048@tmmu.edu.cn
Southwest Hospital
Ge Huang
Affiliated Hospital of Zunyi Medical College
Meiling Tan
Southwest Hospital
Yiqing Xiong
Southwest Hospital
Wei Xiong
Southwest Hospital
Ping Yan
Southwest Hospital
Limeng Dai
Southwest Hospital
Dan Wang
Southwest Hospital

Article

Keywords: ILC3s, Recurrent Pregnancy Loss, Uterine Inflammation, Immune Response, scRNA-seq, RNA-seq

Posted Date: November 12th, 2026

DOI: https://doi.org/10.21203/rs.3.rs-10947166/v1

License: This work is licensed under a Creative Commons Attribution 4.0 International License.
Read Full License

Additional Declarations: No competing interests reported.

Integrated bulk and single-cell transcriptomic profiling identify ILC3s-associated inflammatory signatures in LPS-induced murine pregnancy loss

Yongqin Jia[1#]，Ge Huang[2#]，Meiling Tan[1]，Yiqing Xiong[1]，Wei Xiong[1], Ping Yan[1]，Limeng Dai[1*]，Dan Wang[1*]

[1] Department of Obstetrics and Gynecology, Southwest Hospital, Third Military Medical University (Army Medical University), Chongqing, China.

[2] Department of Gynecology and Obstetrics, The Second Affiliated Hospital of Zunyi Medical University, Zunyi, China.

[*] Corresponding author: Dan Wang, wangdan@tmmu.edu.cn; Limeng Dai, Dailimeng@tmmu.edu.cn.

[#] Yongqin Jia and Ge Huang contributed equally to this work.

Abstract:

Background： RPL is an abnormal pregnancy phenomenon that seriously affects approximately 1%–3% of couples trying to conceive. And accumulating evidence suggests that immune cells disequilibrium at the maternal-fetal interface is a major contributor to unexplained RPL. Among these, group 3 innate lymphoid cells (ILC3s) have been implicated in mucosal immunity, cytokine regulation, and tissue remodeling, yet their role in RPL remains poorly defined.

Methods: In this study, LPS-induced murine miscarriage model was used to evaluate alterations in uterine ILC3s by FC. RNA-seq of uterine samples and scRNA-seq of uterine CD45+ cells were integrated to identify ILC3s-associated clusters and screen DEGs and functional enrichment analyses. Candidate genes were further validated by RT-qPCR in both murine uterine samples and human decidual tissues from RPL cases.

Results： The DEGs from RNA-seq are enriched in inflammatory and cytokine-related pathways. A total of 19021 CD45+ single-cell transcriptomes were captured by scRNA-seq from uterine tissues of LPS-induced pregnancy loss modle and control group, identifying 9 major immune cell populations. Further reclustering of ILC, T, and NK cell compartments demonstrated that the ILC3s subset was enriched in inflammation- and cytokine-related pathways, consistent with bulk RNA-seq findings. Cross-analysis of these pathways identified several shared upregulated genes, which were further validated in both mouse and human samples.

Conclusions： Bluk RNA-seq and single-cell profiling revealed an increased proportion of uterine ILC3s and an ILC3-associated inflammatory transcriptional signature. These findings suggest that ILC3s may be involved in inflammation-related immune remodeling at the maternal–fetal interface and provide a basis for future mechanistic studies.

Keywords: ILC3s; Recurrent Pregnancy Loss; Uterine Inflammation; Immune Response; scRNA-seq; RNA-seq

1. Introduction

Recurrent pregnancy loss (RPL), commonly defined as two or more consecutive spontaneous abortions before 28 weeks of gestation, is a clinically important reproductive disorder affecting approximately 1%–3% of couples of reproductive ages worldwide[1-3]. Despite substantial progress in reproductive medicine, the etiology of RPL remains incompletely understood and are considered multifactorial, involving genetic, anatomical, endocrine, thrombotic, and immunological abnormalities[2]. Among these, immunological dysregulation has been increasingly recognized as a critical contributor to pregnancy failure, especially in unexplained cases. Accumulating evidence suggesting that an imbalance between pro-inflammatory and anti-inflammatory immune responses can impair maternal-fetal tolerance, disrupt embryonic development, and ultimately result in pregnancy loss[4, 5].

Pregnancy success hinges on the establishment of a finely regulated immune equilibrium at the maternal-fetal interface. This delicate balance is sustained through coordinated interactions among multiple immune cell populations, including regulatory T cells (Tregs), uterine natural killer (uNK) cells, macrophages, dendritic cells, and innate lymphoid cells (ILCs) [6, 7]. When this balance becomes disrupted, either excessive inflammatory activation or inadequate immune regulation may compromise decidual homeostasis and trophoblast invasion, thereby predisposing pregnancies to failure[8, 9]. Among ILC subsets, ILC3s have garnered increasing attention for their critical roles in mucosal immunity, inflammatory regulation, and tissue repair. ILC3s are defined by expression of the transcription factor retinoic acid receptor-related orphan receptorγt (RORγt) and their capacity to produce cytokines such as IL-22, IL-17, and GM-CSF[7, 10]. Emerging studies have begun to characterize the distribution and functions of ILC3s within the uterine microenvironment. Uterine ILC3s appear to be dynamically regulated throughout the menstrual cycle and during pregnancy, potentially contributing to endometrial regeneration and local tissue remodeling via cytokine-mediated crosstalk with epithelial and stromal compartments[10, 11]. These findings suggest that aberrant activation or redistribution of ILC3s may disturb immune homeostasis at the maternal-fetal interface and consequently contribute to RPL pathogenesis.

While pregnancy-related ILC3s have been examined, the single-cell characteristics of ILC3s in inflammation-induced pregnancy loss, particularly in RPL, remain to be defined. To investigate how immune disturbance affects uterine ILC3s during early pregnancy, we employed an LPS-induced

abortion model in combination with bulk RNA-seq and scRNA-seq to systematically profile transcriptional features and subset alterations of ILC3s at the maternal-fetal interface. Our study aims to elucidate the critical role of ILC3s in inflammation-mediated pregnancy loss and immune regulation, offering new insights into the immunopathological mechanisms underlying RPL.

2. Materials and methods

2.1 Animals and LPS-induced pregnancy loss model

Female and male C57BL/6J mice (8 weeks, 18–25g) were purchased from GemPharmatech Co. Ltd. (chengdu, China) and raised in a specific pathogen free (SPF) facility at the Laboratory Animal Centre of Southwest Hospital, Third Military Medical University (Chongqing, China). LPS was purchased from Solarbio (Cat. No. L8880), derived from serotype Escherichia coli O55: B5 and extracted using the benzene method. 10mg LPS powder dissolved in 1ml PBS, with a storage concentration of 10mg/ml, and a usage concentration of 2.0ug/100ul. After mating, pregnant mice were randomly assigned to the experimental or control group at gestational 6.5d (G6.5) and 8.5d (G8.5), respectively. Mice in the experimental group received an intraperitoneal injection of LPS at a dose of 2.0μg diluted in 100μl PBS, whereas control mice received an equal volume of PBS alone. Embryo resorption was assessed 24h (G7.5 and G9.5) after injection based on gross morphology of implantation sites, and uterine tissues were collected for subsequent analyses. Subsequently, mice were euthanized via cervical dislocation until loss of corneal reflex was confirmed.

2.2 Isolation of uterine cells and flow cytometric analysis of ILC3s

Fresh uterine tissues were harvested from pregnant mice, minced into small fragments, and digested in DMEM containing collagenase IV and hyaluronidase at 37°C on an orbital shaker for 1h. The resulting cell suspension was filtered through a 70-μm cell strainer to obtain single cells. Uterine ILC3s were identified as Lin−CD45+Thy1.2+RORγt+ cells, cell viability was assessed using Fixable Viability Stain 700 (Fvs700) (564997, BD Pharmingen). Living cells were stained with fluorochrome-conjugated antibodies diluted 1:100 in PBS, including Lineage Antibody Cocktail (561317, BD Pharmingen), anti-CD45 (561037, BD Pharmingen), anti-Thy1.2 (105311, BioLegend), and anti-RORγt (564722, BD Pharmingen). Furthermore, Lineage Antibody Cocktail, which components include CD3e, CD11b, B220, TER-119, GR-1. Multicolor flow cytometric analysis was performed using a BD FACSCelesta instrument, and data were analyzed with FlowJo software (version 10.9.0). Uterine ILC3s were identified according to the gating strategy described

in the corresponding figure legends.

2.3 RNA-sequencing

For bulk RNA sequencing, pregnant mice were intraperitoneally injected with LPS at gestational 8.5d (G8.5), and uterine tissues were collected 24h later (G9.5). Total RNA was extracted from uterine tissues and submitted to Majorbio Bio-Pharm Technology Co., Ltd. (Shanghai, China) for library construction and RNA sequencing.

2.4 scRNA-seq processing and quality control

For scRNA-seq, pregnant mice were intraperitoneally injected with LPS at gestational 8.5d, and fresh uterine tissues were collected 24h later (G9.5) and immediately transferred to Majorbio Bio-Pharm Technology Co., Ltd. for sample processing. To capture more signal cells, uterine CD45+ cells from three mice per group were pooled before library construction. Preparation of single-cell suspensions and sorting of CD45+ immune cells were performed by trained technicians at the sequencing facility. Raw scRNA-seq data were processed using the standard analysis pipeline provided by the sequencing platform. The scRNA-seq analysis was performed with the Cell Ranger v9.0.0 software using the default parameters. The number of CD45+ cells estimated in each group of samples were 8546 and 10475, and mean reads per cell were 41609 to 35096, respectively. Cells with extremely low number of UMI counts were filtered out. Quality control filtering was applied to each sample to eliminate downstream analysis of empty droplets, low-quality cells, and potential doublets using DoubletFinder. Data normalization, variable feature selection, scaling, PCA, clustering and UMAP visualization were performed using Seurat, the resolution is defined as 0.8. The number of genes detected in each cell (nFeature_RNA), the total number of molecules detected within a cell (nCount_RNA), and the percentage of reads that map to the mitochondrial genome were calculated and showed in Fig.S1 (Supplementary Table 1.). Cell clusters were annotated based on canonical marker genes and reference databases including Mouse Cell Atlas, CellMarker and PanglaoDB.

2.5 Differential expression and functional enrichment analyses

DEGs identified from both bulk RNA-seq and scRNA-seq datasets were screened using the criteria of $|\log2FC| \geq 1$ and $P<0.05$. Genes with $\log2FC > 1$ were considered as upregulated, whereas genes with $\log2FC < -1$ were considered as downregulated. Volcano plots and heatmaps were generated to visualize the differential expression profiles. To further explore the potential biological

functions and signaling pathways associated with these DEGs, Gene Ontology (GO) term analysis and Kyoto Encyclopedia of Genes and Genomes (KEGG) pathway analysis were performed using the Database for Annotation, Visualization and Integrated Discovery (DAVID, https://david.ncifcrf.gov/)[12]. In the GO term analysis including biological processes (BP), cellular components (CC) and molecular functions (MF); $p<0.05$ was considered statistically significant.

2.6 Gene set enrichment analysis (GSEA)

GSEA was performed to further evaluate biological processes and pathways differentially enriched between the control and LPS-treated groups. GSEA was conducted using the Majorbio Cloud platform(www.majorbio.com) based on ranked gene expression data. Enrichment scores were calculated using a weighted Kolmogorov–Smirnov-like statistic, which reflects the degree to which a predefined gene set is overrepresented at the top or bottom of the ranked gene list[13, 14]. Gene sets with significant enrichment were considered to be associated with the corresponding phenotype.

2.7 Collection of human decidual samples

This study adhered to the Declaration of Helsinki, and all tissue samples and data were obtained with informed consent before inclusion in the study and were approved by the Ethics Committee of the First Affiliated Hospital of Army Medical University (Approval number: (A)KY2024212). All patients signed informed consent before inclusion in the study. Human decidual tissues were obtained from women with RPL and gestational age-matched controls, including 7 normal samples and 12 RPL samples, all of whom underwent selective termination surgery for normal early pregnancy. RPL was defined as two or more consecutive spontaneous abortions before 28 weeks of gestation. Patients with chromosomal abnormalities, uterine malformations, antiphospholipid syndrome, endocrine disorders or active infection were excluded.

2.8 RT-qPCR Validation

According to manufacturer's instructions, total RNA was isolated from uterine tissues of RPL and control pregnant mice by using TRIzol reagent (TAKARA, Japan) and further reverse transcribed to cDNA with PrimeScript^{TM} FAST RT reagent Kit with gDNA Eraser (TAKARA, Japan). RT-qPCR was performed using SupRealQ Ultra Hunter SYBR qPCR Master Mix (Vazyme, Nanjing) on CFX Connect Real Time System (Bio-Rad, USA). Relative gene expression levels were normalized to GAPDH and calculated with the $2^{-\Delta\Delta Ct}$ method, data acquisition was carried out with Bio-Rad CFX Manager software and analyzed using GraphPad prism 9.5.0. At least three

independent biological replicates were included in each experiment. Primer sequences were listed in Supplementary Table 2.

2.9 Data analysis and statistics

Statistical analyses were conducted with GraphPad prism (version 9.5, USA). Data are presented as mean ± SEM unless otherwise indicated. Normality was assessed before statistical comparisons. For two-group comparisons, unpaired Student's t-test or Mann–Whitney U test was used as appropriate.

3. Results

3.1 Uterine ILC3s were increased in the LPS-induced pregnancy loss model during early pregnancy

To investigate the function of ILC3s in LPS-induced pregnancy loss model during early pregnancy, non-pregnant mice and pregnant mice were intraperitoneally treated with PBS or LPS at G6.5 and G8.5, each group consists of 3 mice. The experimental scheme is shown in Fig. 5A. Compared with PBS-treated controls, LPS-treated mice showed obvious embryo resorption and increased resorption rates 24h after injection (Fig.1B), statistical chart of embryo absorption rate is shown in Fig.1C. Uterine tissues were harvested 24h after treatment, dissociated into single-cell suspensions, and analyzed by FC. Uterine ILC3s were identified as Lin−CD45+Thy1.2+RORγt+ cells, and FC results showed that the proportion of uterine ILC3s changed dynamically during early pregnancy and in response to inflammatory challenge. Compared with non-pregnant mice, the proportion of ILC3s tended to increase during early pregnancy, with the lowest in non-pregnant mice and the highest at G9.5; More importantly, LPS treatment significantly increased the proportion of uterine ILC3s at G9.5, whereas, there was no statistically significant difference in the relative abundance of ILC3s when non-pregnant and G7.5 between LPS treatment and control mice (*P < 0.05, **P<0.01; Fig.3D, E). These data indicate that uterine ILC3s excessive accumulated in the LPS-induced pregnancy loss model, supporting a potential role for this cell population in the pathological process of pregnancy loss.

3.2 LPS-induced pregnancy loss model exhibited activation of immune-related responses

The mice gestation 8.5d were intraperitoneally injected with LPS, and uterine tissues were collected 24h later for transcriptomic analysis (Fig. 2A). RNA-seq analysis identified a total of

3,494 DEGs between RPL and control groups according to the criteria of |log2FC|≥1 and $P < 0.05$, including 1,678 upregulated and 1,816 downregulated genes, the volcano plots and heat maps of DEGs were shown (Fig.2B-C). To further characterize the biological processes associated with LPS-induced pregnancy loss, GO and KEGG enrichment analyses were performed with identified DEGs[14, 15]. These analyses revealed significant enrichment of multiple immune- and inflammation-related pathways, including cytokine-cytokine receptor interaction, viral protein interaction with cytokine and cytokine receptor, TNF signaling, and IL-17 signaling (Fig. 2D, E, Supplementary Table 3). Consistent with these findings, GSEA further demonstrated significant enrichment of gene sets associated with activation of innate immune response, activation of immune response, and immune response-regulating signaling pathways in the RPL group (Fig. 2F). Collectively, these results indicated that LPS-induced pregnancy loss model is accompanied by robust activation of multiple immune and inflammatory responses.

3.3 Single-cell transcriptomic analysis revealed substantial remodeling of uterine CD45+ immune cell populations in LPS-induced pregnancy loss

Previous studies have shown that dysfunction of various immune cell populations contributes to the development of RPL [16], including abnormalities in decidual natural killer (dNK) cells[7], imbalance of T-cell subsets[17], and excessive activation of pro-inflammatory macrophages[18]. To further define the immune alterations associated with RPL, we performed scRNA-seq analysis of uterine CD45+ cells isolated from LPS-induced pregnancy loss and control mice (Fig.3A). Uniform Manifold Approximation and Projection (UMAP) visualization demonstrated marked differences in the composition of uterine immune cells between the two groups (Fig.3B, C). Compared with controls, the proportion of neutrophils, T cells, ILCs were increased in the RPL group, whereas macrophage-monocyte, DCs, and NK cells were reduced. To obtain higher-resolution information on lymphoid subsets, ILCs, T cells and NK cells were extracted for reclustering analysis. This analysis identified 8 subpopulations, including NK cells, type 3 innate lymphoid cells (ILC3s), γδT cells, TSTR cells, CD4+ memory T cells, CD4+ naive T cells, CD8+ effector T cells, NK T cells (Fig.3D). The definitions of all cell subpopulations referred to the public databases (Mouse Cell Atlas, Cell Marker and Panglao DB) and previous reports. Among these subsets, ILC3s were defined as Rorc+ cells expressing Il17a and/or Il22 (Fig.3E). Quantitative analysis further showed pronounced changes in the abundance of these immune cell subsets in the RPL uterus (Fig.3F).

These findings suggest that LPS-induced pregnancy loss is associated with extensive remodeling of the uterine immune microenvironment.

3.4 ILC3 accumulation in RPL was associated with activation of inflammatory and cytokine-related pathways

To explore the molecular mechanism of ILC3s in RPL, we further analyzed the scRNA-seq profiles of uterine ILC3s cells from the RPL and control group. Using a cutoff of $|\log2FC| \geq 0.5$ and $P<0.05$, a total of 724 DEGs were identified, including 340 upregulated genes and 384 downregulated genes in ILC3s from RPL-like model (Fig. 4A). The top 10 DEGs were shown in the heatmap (Fig.4B), including S100a8, Lcn2, Retnlg, S100a9, G0s2, Wfdc21, Ngp, H2-Eb1, H2Aa, Cd74. To verify the scRNA-seq results, RT-qPCR was performed to identified the expression of DEGs (Fig.4C). Functional enrichment analysis revealed that these ILC3s-associated DEGs were mainly involved in immune- and inflammation-related processes. GO analysis showed significant enrichment in biological processes such as innate immune response and cytokine activity (Fig.4D), and KEGG analysis identified enrichment in canonical inflammatory pathways, including the IL-17 signaling pathway, TNF signaling pathway, and cytokine-cytokine receptor interaction (Fig.4E). These results were largely consistent with the bulk RNA-seq findings. To identify candidate genes that are simultaneously involved in the overall uterine inflammatory response and enriched in ILC3s, we integrated DEGs from 4 common pathways between scRNA-seq and bulk RNA-seq datasets. A total of 33 overlapping genes were identified through this integrated approach (Fig.4F). The 33 overlapping genes involved pathway were shown in Fig.4G.

To investigate the relationships among these overlapping genes, we constructed a gene co-expression network by String database (https://cn.string-db.org/) and visualized it through Cytoscapes (Fig.5A-B). Further module analysis based on MCODE algorithm and degree centrality revealed a highly interconnected subnetwork. A total of 15 DEGs were identified from the MCODE1 cluster (15nodes 101edges), and overlapping genes were obtained by intersecting these with the top 15 DEGs screened by degree centrality analysis (Fig.5C-D). Among of this, 13 overlaping genes were screened and these 13 hub genes may play critical roles in transcriptional regulatory programs associated with ILC3s. Notably, violin plot analysis showed that 7 hub genes identified by MCODE and degree centrality were expressed at markedly higher levels in the ILC3 subset than in other immune cell subsets (Fig.5E), another 6 hub genes were identified from the ILC3-associated DEGs

set, their expression was not exclusively restricted to ILC3s, suggesting that they may represent a broader inflammatory gene program shared by multiple immune cell populations (Fig.S2).

Interactions among TFs, miRNAs and hub genes are considered as an important way to verify the hub genes expression changes at transcriptional and post-transcriptional levels. In the miRNA-hub genes-TFs coregulatory network, hub gene expression can be regulated by TF-genes and miRNAs. The network contained 6 target genes, regulated by 28 miRNAs and 29 TF-genes, among which Mmp9 was modulated by the greatest number of miRNAs and TFs (Fig.5F). This regulatory network was based on bioinformatic prediction and requires further experimental validation. Together, these findings establish a foundation for confirming the presence of an ILC3-enriched inflammatory gene network in RPL, indicating that ILC3s may contribute to disease progression through the coordinated regulation of cytokine and chemokine-related signaling pathways.

3.5 Hub genes of ILC3s were validated in mice uterine and human decidual tissues

The expression patterns of hub genes identified by transcriptomic analysis, we performed RT-qPCR on mouse uterine tissues and human decidual tissues from RPL samples. Overall, the expression profiles of most hub genes were concordant between mouse uterine and human decidual tissues (Fig. 6A, B). By contrast, CXCL2 and CXCL3 showed no statistically significant alterations in human decidual tissues, which may reflect the limited sample size available. These findings offer cross-species support for the involvement of the identified hub genes in RPL-associated immune dysregulation.

4. Discussion

To characterize uterine ILC3s phenotypes under inflammatory conditions during early pregnancy and investigate their potential involvement in RPL, we employed an LPS-induced abortion mouse model. While this experimental system cannot completely model the multifactorial etiologies underlying human RPL—a condition affecting approximately 1% to 2% of women of reproductive age—it offers a valuable approach for examining inflammation-mediated pregnancy loss. Our data demonstrate that LPS treatment remodeled the uterine immune microenvironment, characterized by enrichment of ILC3 populations and upregulation of inflammatory signaling cascades. ScRNA sequencing and bulk RNA-seq integration revealed an ILC3-specific gene signature enriched for cytokine-mediated responses and innate immune activation pathways. Collectively, our results indicate that uterine ILC3s participate in inflammation-associated immune remodeling during

pregnancy failure; however, whether these cells directly drive pregnancy loss requires further investigation.

Accumulating evidence indicates that innate lymphoid cells are important regulators of immune homeostasis at the maternal-fetal interface[7]. In normal pregnancy, ILC3s are mainly distributed around the endometrium and uterine glands, and maintain the homeostasis and remodeling of placental tissue by secreting cytokines such as IL-22, IL-17, GM-CSF, and IL-8[19]. Because ILC3s display considerable functional plasticity, they may support either tissue repair or inflammatory activation depending on the surrounding microenvironment. This dual nature is particularly relevant during pregnancy, when immune tolerance and host defense must remain tightly balanced[10, 20]. Previous studies have suggested that decidual ILC3s subsets may interact with stromal, epithelial, endothelial, and myeloid cells to support tissue homeostasis and vascular adaptation, whereas dysregulated activation of these cells may disturb maternal-fetal immune tolerance[21, 22]. However, the present study does not establish whether ILC3s are primary drivers of embryo resorption or secondary responders to LPS-induced inflammation. Functional perturbation experiments, including ILC3 depletion, RORγt inhibition, or blockade of IL-17/IL-22-related pathways, will be required to clarify the causal role of ILC3s in pregnancy loss.

In our study, LPS treatment resulted in a marked increase in uterine ILC3s abundance together with enhanced expression of inflammatory genes and enrichment of pathways related to cytokine-cytokine receptor interaction, TNF signaling, and IL-17 signaling. These findings support the idea that ILC3s shift toward pro-inflammatory state under pathological conditions. Although cytokines such as IL-17 and IL-22 may contribute to normal tissue remodeling and barrier maintenance during pregnancy, dysregulation of these mediators in an inflammatory setting may amplify local immune activation and compromise placental homeostasis[23]. In this context, our observation that hub genes such as Il1b, Il1rn, Cxcl2, and Ccr1 were enriched in ILC3s, suggests that these cells may participate in the recruitment and activation of other immune populations, thereby reinforcing the inflammatory cascade in the uterus. An additional point worth noting is the potential heterogeneity of ILC3 subsets during pregnancy. NCR+ and NCR- ILC3s may exert distinct, and in some contexts even opposing functions. Experimental evidence suggests that NCR+ ILC3s may display reduced antigen-presenting potential under low-oxygen conditions, the feature may be relevant to fetal tolerance, whereas other ILC3 states may be more closely linked to inflammatory effector

responses[24]. Moreover, decidual NCR+ ILC3s have been described as a predominant human decidual ILC3 population with a characteristic immune-regulatory profile[25]. Therefore, the proportion increase of ILC3s observed in our model may reflect a shift not only cell number but also ILC3s subset composition and functional state. This may help explain how ILC3s, which are potentially beneficial in physiological pregnancy, become pathogenic in an inflammation-driven miscarriage setting.

Our findings suggest potential translational relevance. Given that ILC3s appear to occupy a pivotal position at the convergence of immune tolerance, cytokine signaling, and tissue remodeling，they may constitute a viable therapeutic target for immune-mediated pregnancy loss[25]. Rather than broadly suppressing inflammatory responses, future therapeutic strategies may need to focus on restoring functional homeostasis of ILC3s and their downstream signaling networks.

This study has several limitations. First, the LPS-induced abortion model primarily reflects acute inflammation triggered by bacterial endotoxin and may not fully recapitulate the heterogeneous mechanisms underlying RPL, particularly non-infectious or idiopathic forms. Further investigation is warranted to elucidate the role of ILC3s in non-infectious RPL models. Second, the use of pooled samples for scRNA-seq precluded comprehensive assessment of inter-individual variation. Third, functional differences among ILC3 subsets were not examined in sufficient depth, particularly between NCR+ and NCR− populations, which may harbor distinct immunoregulatory roles at the maternal-fetal interface. Finally, although several hub genes were validated in both murine and human tissues, the human sample size remained limited. Additional validation in larger, independent clinical cohorts is necessary to confirm these findings.

In summary, our study demonstrates that uterine ILC3s undergo substantial quantitative and transcriptional changes in an LPS-induced miscarriage model and suggests that these cells may contribute to immune imbalance at the maternal-fetal interface. By linking ILC3s expansion to cytokine-associated signaling and intercellular communication networks, our findings provide additional insight into the immune mechanisms of pregnancy loss and identify ILC3s-related pathways as potential candidates for future mechanistic and translational studies.

Ethical approval and consent to participate

The studies involving human participants were reviewed and approved by the Research and

Clinical Trial Ethics Committee of the First Affiliated Hospital of Army Medical University. The patients provided their written informed consent to participate in this study (Approval number: (A)KY2024212). Animal’s experiments were performed in accordance with the Laboratory Animal Welfare and the study was approved by the Ethics Committee of the Army Medical University (Approval number: AMUWEC20262049).

Consent for publication

All authors critically reviewed the manuscript and contributed to the final manuscript. All authors approved this manuscript for publication.

Data availability

The data of RNA-seq in this study are available from https://www.ncbi.nlm.nih.gov/geo/query/acc.cgi?acc=GSE349426.

Enter token: wrydmukypnublwl

The data of scRNA-seq in this study are available from https://www.ncbi.nlm.nih.gov/geo/query/acc.cgi?acc=GSE349586.

Enter token: wnsxcgygtxehdsz "

Conflicts of Interest

The authors declare that they have no known competing financial interests or personal relationships that could have appeared to influence the work reported in this paper.

Authors’ Contributions

Dan Wang conceptualized the study and reviewed, and edited the manuscript. Limeng Dai was in charge of supervision and edited the manuscript. Yongqin Jia and Ge Huang worked on the animal experiment, data curation and wrote the original draft preparation. Meiling Tan and Ping Yan was in charge of the visualization of scRNA-seq and RNA-seq. Yiqing Xiong and Wei Xiong carried out the samples collected and RT-qPCR. Yongqin Jia and Ge Huang contributed equally to this work.

Funding

This research was supported by the Natural Science Foundation Project of Chongqing (grant number CSTB2022NSCQ-MSX0169) and Science and Technology Program Project of Chongqing

(grant number CSTB2022TIAD-KPX0173).

Acknowledgements

Not applicable.

References

[1] M.F. Diejomaoh, Recurrent spontaneous miscarriage is still a challenging diagnostic and therapeutic quagmire, Med Princ Pract, 24 Suppl 1 (2015) 38-55.

[2] E.G.G.o. RPL, R. Bender Atik, O.B. Christiansen, J. Elson, A.M. Kolte, S. Lewis, S. Middeldorp, S. McHeik, B. Peramo, S. Quenby, H.S. Nielsen, M.L. van der Hoorn, N. Vermeulen, M. Goddijn, ESHRE guideline: recurrent pregnancy loss: an update in 2022, Hum Reprod Open, 2023 (2023) hoad002.

[3] A. Bosire, R. Kosgei, D. Gathara, M. Madadi, A. Osoti, Burden, causes, and treatment approaches of recurrent pregnancy loss: a scoping review, Pan Afr Med J, 52 (2025) 109.

[4] J.S. Joo, D. Lee, J.Y. Hong, Multi-Layered Mechanisms of Immunological Tolerance at the Maternal-Fetal Interface, Immune Netw, 24 (2024) e30.

[5] I. Cuadrado-Torroglosa, J.A. Garcia-Velasco, D. Alecsandru, Maternal-Fetal Compatibility in Recurrent Pregnancy Loss, J Clin Med, 13 (2024).

[6] X. Ma, X. Chen, X. Mu, M. Cao, Y. Zhang, Epigenetics of maternal-fetal interface immune microenvironment and placental related pregnancy complications, Front Immunol, 16 (2025) 1549839.

[7] R.Q. Chang, W.J. Zhou, D.J. Li, M.Q. Li, Innate Lymphoid Cells at the Maternal-Fetal Interface in Human Pregnancy, Int J Biol Sci, 16 (2020) 957-969.

[8] Z. Liu, Y. Geng, Y. Huang, R. Hu, F. Li, J. Ding, W. Ma, H. Dong, K. Song, X. Xu, X. Wu, Y. Song, M. Zhang, Bushen Antai recipe alleviates embryo absorption by enhancing immune tolerance and angiogenesis at the maternal-fetal interface via mobilizing MDSCs in abortion-prone mice, Phytomedicine, 123 (2024) 155164.

[9] Y. You, P. Stelzl, D.N. Joseph, P.B. Aldo, A.J. Maxwell, N. Dekel, A. Liao, S. Whirledge, G. Mor, TNF-alpha Regulated Endometrial Stroma Secretome Promotes Trophoblast Invasion, Front Immunol, 12 (2021) 737401.

[10] J. Mendes, A.L. Areia, P. Rodrigues-Santos, M. Santos-Rosa, A. Mota-Pinto, Innate Lymphoid Cells in Human Pregnancy, Front Immunol, 11 (2020) 551707.

[11] U. Ganieva, S. Schneiderman, P. Bu, K. Beaman, S. Dambaeva, IL-22 regulates endometrial regeneration by enhancing tight junctions and orchestrating extracellular matrix, Front Immunol, 13 (2022) 955576.

[12] B.T. Sherman, M. Hao, J. Qiu, X. Jiao, M.W. Baseler, H.C. Lane, T. Imamichi, W. Chang, DAVID: a web server for functional enrichment analysis and functional annotation of gene lists (2021 update), Nucleic Acids Res, 50 (2022) W216-W221.

[13] A. Subramanian, P. Tamayo, V.K. Mootha, S. Mukherjee, B.L. Ebert, M.A. Gillette, A. Paulovich, S.L. Pomeroy, T.R. Golub, E.S. Lander, J.P. Mesirov, Gene set enrichment analysis: A knowledge-based approach for interpreting genome-wide expression profiles, Proc. Natl. Acad. Sci. U. S. A., 102 (2005) 15545-15550.

[14] M. Kanehisa, S. Goto, KEGG: kyoto encyclopedia of genes and genomes, Nucleic Acids Res, 28 (2000) 27-30.

[15] M. Kanehisa, Y. Sato, M. Kawashima, M. Furumichi, M. Tanabe, KEGG as a reference resource for gene and protein annotation, Nucleic Acids Res, 44 (2016) D457-D462.

[16] D. Miller, K. Motomura, V. Garcia-Flores, R. Romero, N. Gomez-Lopez, Innate Lymphoid Cells in the Maternal and Fetal Compartments, Front Immunol, 9 (2018) 2396.
[17] X. Zhao, Y. Jiang, L. Wang, Z. Li, Q. Li, X. Feng, Advances in Understanding the Immune Imbalance between T-Lymphocyte Subsets and NK Cells in Recurrent Spontaneous Abortion, Geburtshilfe Frauenheilkd, 78 (2018) 677-683.
[18] M. Lin, H. Xu, J. Qiu, Inflammation in recurrent miscarriage - a comprehensive perspective from uterine microenvironment and immune cell imbalance to therapeutic strategies, Ginekol Pol, 95 (2024) 266-275.
[19] P. Vacca, C. Vitale, E. Munari, M.A. Cassatella, M.C. Mingari, L. Moretta, Human Innate Lymphoid Cells: Their Functional and Cellular Interactions in Decidua, Front Immunol, 9 (2018) 1897.
[20] J.M. Murphy, L. Ngai, A. Mortha, S.Q. Crome, Tissue-Dependent Adaptations and Functions of Innate Lymphoid Cells, Front Immunol, 13 (2022) 836999.
[21] O. Huhn, X. Zhao, L. Esposito, A. Moffett, F. Colucci, A.M. Sharkey, How Do Uterine Natural Killer and Innate Lymphoid Cells Contribute to Successful Pregnancy?, Front Immunol, 12 (2021) 607669.
[22] M.P. Piccinni, R. Raghupathy, S. Saito, J. Szekeres-Bartho, Cytokines, Hormones and Cellular Regulatory Mechanisms Favoring Successful Reproduction, Front Immunol, 12 (2021) 717808.
[23] L.J. Yockey, A. Iwasaki, Interferons and Proinflammatory Cytokines in Pregnancy and Fetal Development, Immunity, 49 (2018) 397-412.
[24] R. Einenkel, J. Ehrhardt, M. Zygmunt, D.O. Muzzio, Oxygen regulates ILC3 antigen presentation potential and pregnancy-related hormone actions, Reprod Biol Endocrinol, 20 (2022) 109.
[25] J. Mendes, P. Rodrigues-Santos, A.L. Areia, J.S. Almeida, V. Alves, M. Santos-Rosa, A. Mota-Pinto, Type 2 and type 3 innate lymphoid cells at the maternal-fetal interface: implications in preterm birth, Bmc Immunol, 22 (2021) 28.

Figures:

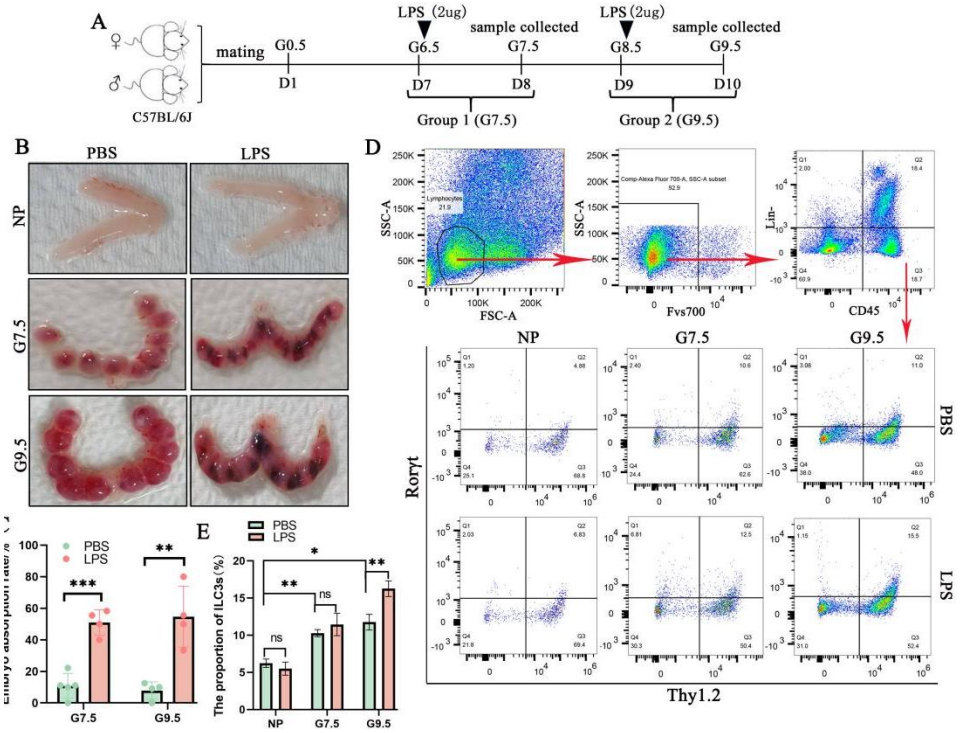


Figure1：Flow cytometric validation of uterine ILC3 accumulation after LPS treatment. (A) Schematic representation of the experimental setup. (B-C) Representative images and quantification of embryo resorption after LPS or PBS treatment. (D) Gating strategy for identification of uterine ILC3s by FC，ILC3s defined as Lin−CD45+Thy1.2+RORγt+(n=3). (E) Quantification of the proportion of uterine ILC3s determined by FC. *P < 0.05, **P < 0.01, ***P < 0.001, ns.P>0.05.

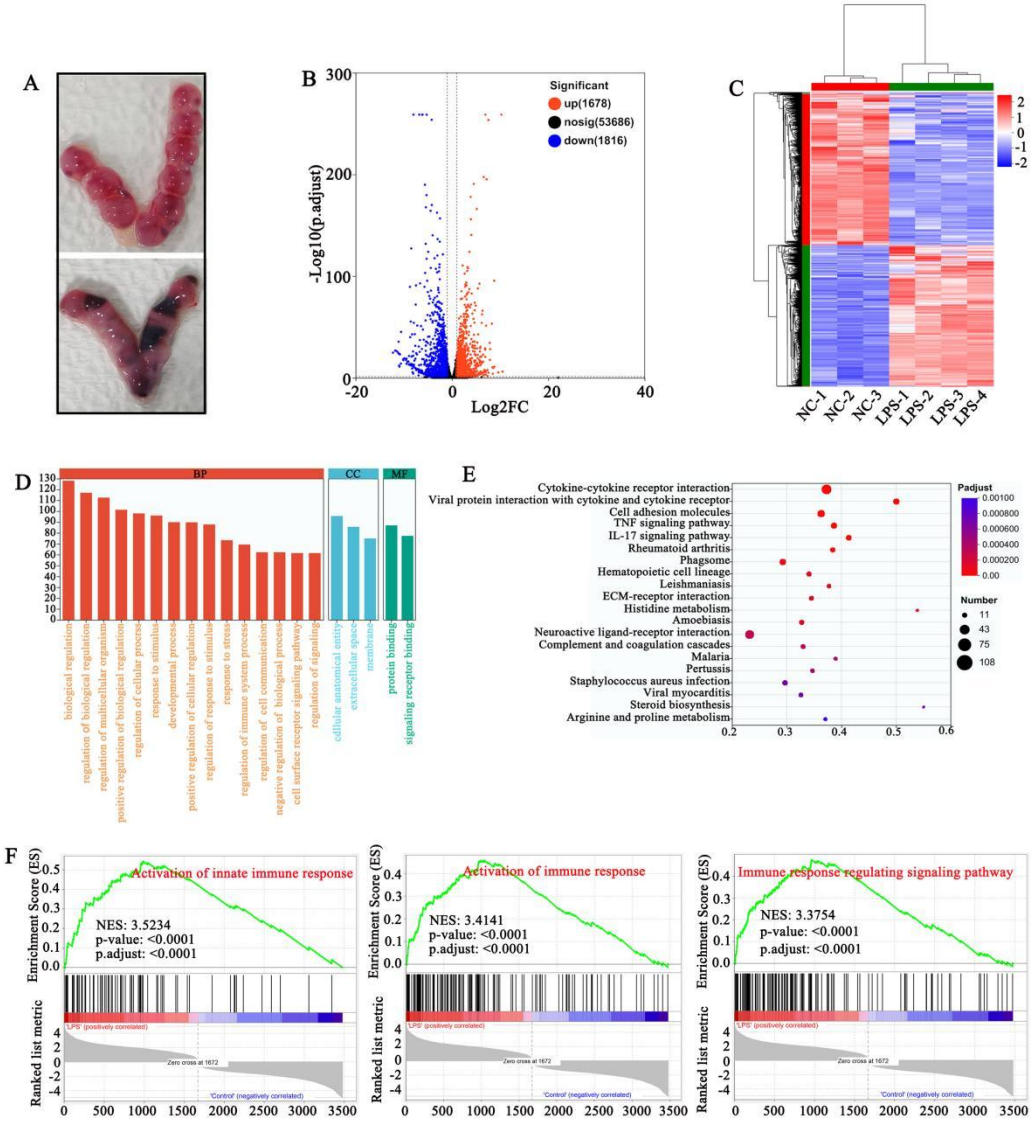


Figure 2：LPS-induced pregnancy loss and activation of immune-related transcriptional responses in the uterus. (A) Representative images showing embryonic loss after LPS or PBS injection. (B–C) Volcano plots and heatmaps of DEGs between LPS-treated and control groups. (D–E) GO term and KEGG enrichment analyses of DEGs. (F) GSEA-based GO enrichment plots for selected gene sets, including activation of innate immune response, activation of immune response, and immune response–regulating signaling pathways. In the enrichment plots, the x-axis denotes ranked genes, with vertical black lines indicating gene positions within the specified gene sets. The y-axis represents the normalized enrichment score. Red and blue regions indicate positive and negative correlations, respectively.

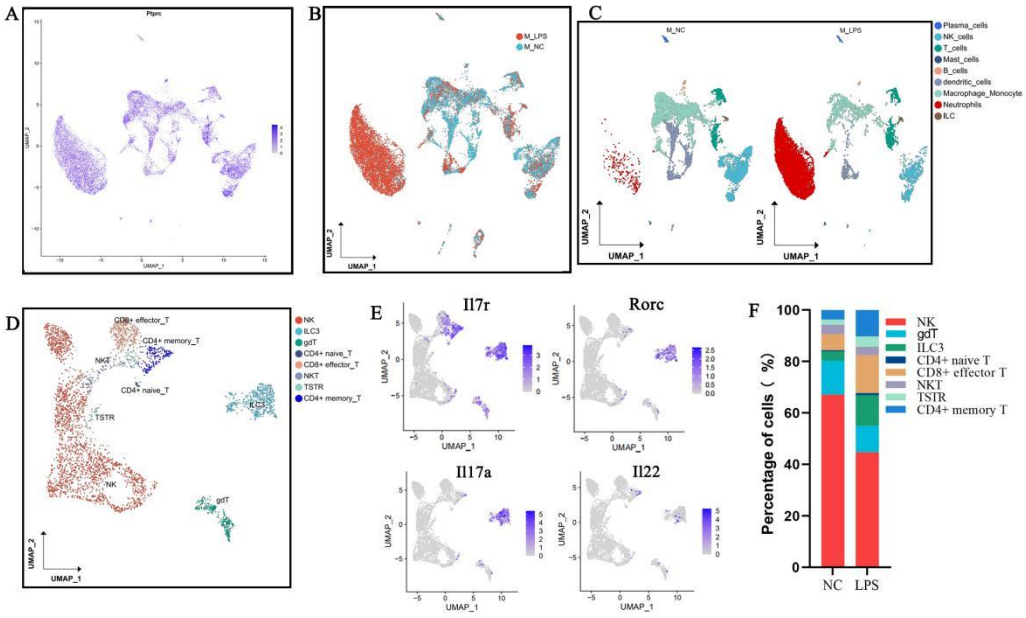


Figure3：Single-cell transcriptomic atlas of uterine CD45+ immune cells from LPS-treated and control mice. (A) UMAP visualization of dimensionality reduction clustering plot CD45+ cells; (B) UMAP visualization of CD45+ immune cells from the two groups. (C) Annotation of 9 immune cell populations based on marker genes with SingleR and CellMarker. (D) UMAP plot showing reclustering of ILCs, T cells, and NK cells. (E) Feature plots showing expression of representative marker genes for the ILC3s subset. (F) Relative proportions of the major immune cell populations in the control and LPS-treated groups.

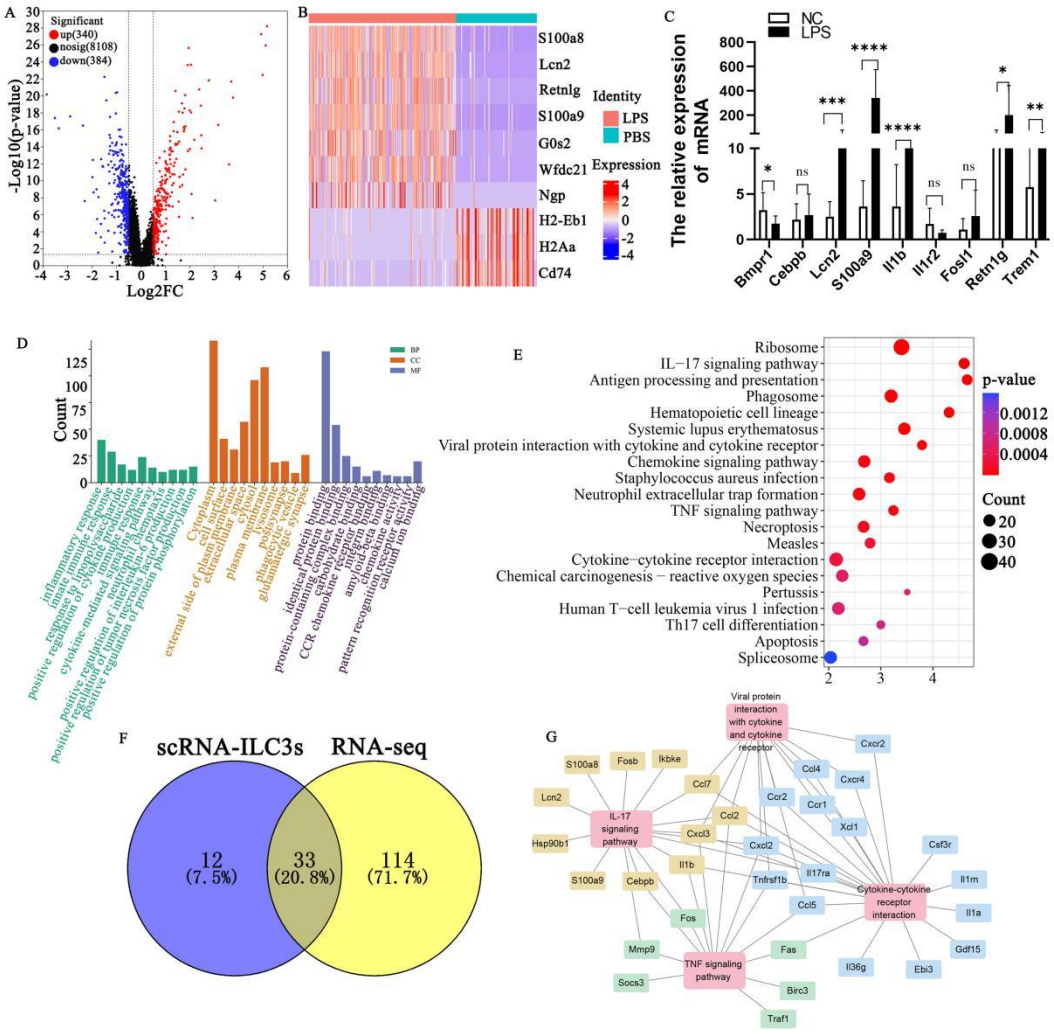


Figure4: Identification of ILC3s-associated hub genes based on integrated transcriptomic analysis. (A-B) The volcano plots and heat maps of DEGs in uterine ILC3s identified by scRNA-seq. (C) RT-qPCR was performed to validate the mRNA expression of DEGs. (D-E) GO term and KEGG enrichment analyses of ILC3-associated DEGs. (F) Venn diagram showing overlapping genes identified in immune-related pathway from RNA-seq and scRNA-seq datasets. (G) Gene-network plot of KEGG pathway enrichment analysis of hub genes. *P < 0.05, **P < 0.01, ***P < 0.001, ****P < 0.0001, ns.P>0.05.

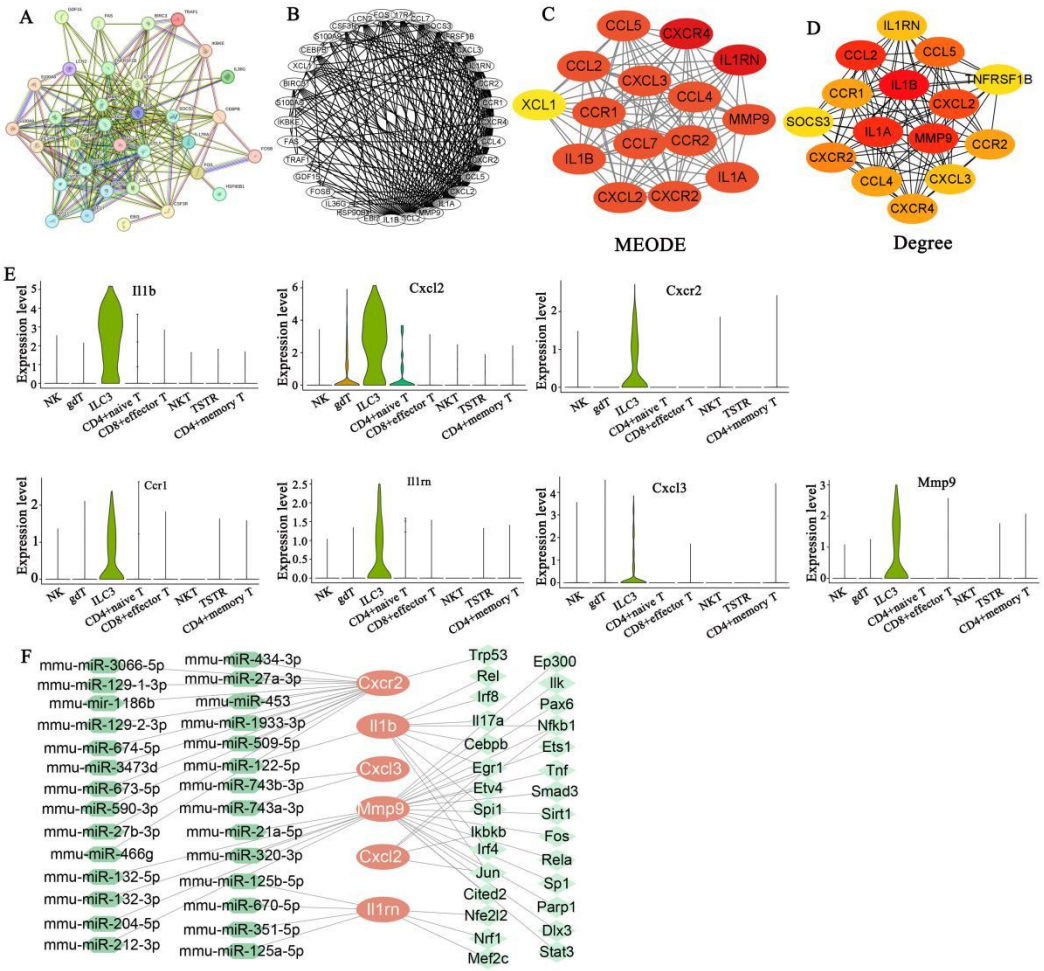


Figure5: The construction of PPI networks and TFs-hub genes-miRNAs networks. (A-B) The PPI network of overlapping genes constructed using the STRING database and visualized in Cytoscape. (C-D) Identification of hub genes from the PPI network based on MCODE analysis and degree centrality. (E) The violin plots showing the expression of hub genes in ILC3s and other immune cell populations. (F) TFs-hub genes-miRNAs co-regulatory network identification. There were 28 miRNAs (left) and 29 TF genes (right) in the network, and they interacted with 6 hub genes (red).

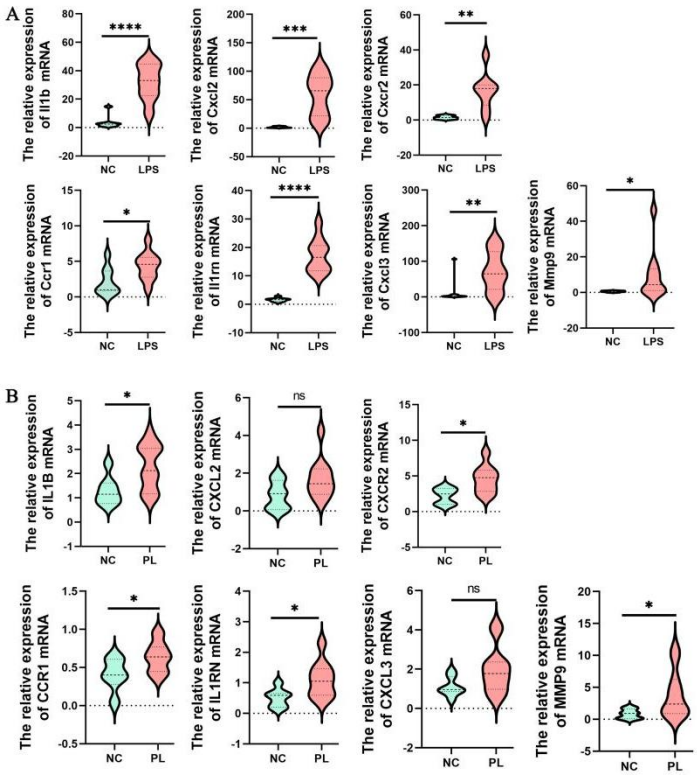


Figure 6：Validation of hub gene expression in mouse uterine and human decidual tissues. (A) Relative mRNA expression levels of hub genes in mouse uterus tissues; (B) Relative mRNA expression level of hub genes in human decidual tissues. *P < 0.05, **P < 0.01, ***P < 0.001, ****P < 0.0001, ns.P>0.05.

Supplementary Figures

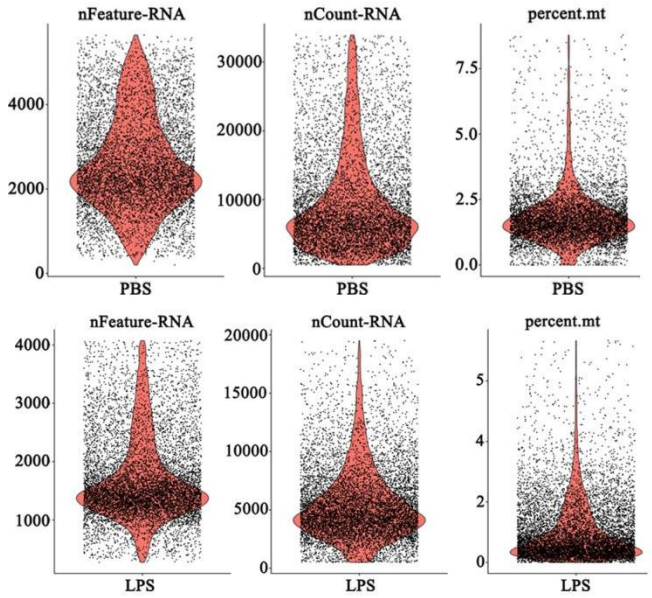


Fig.S1. Post quality control filtering of each sequenced cell, which was plotted in violin plots to display their number of nFeature-RNA, absolutenCount-RNA, and the percentage of mitochondria (percent.mt).

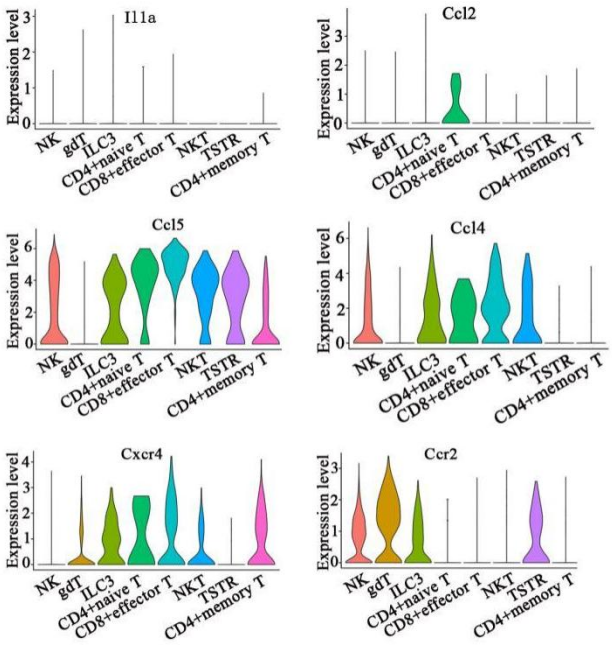


Fig.S2. Violin plots showing the expression distribution of 6 hub genes across ILC3s and other immune cell populations.

Supplementary Files

This is a list of supplementary files associated with this preprint. Click to download.

- supplementary.xlsx